

Surface Plasmons Reveal Spin Crossover in Nanometric Layers

Gautier Félix,[†] Khaldoun Abdul-Kader,[†] Tarik Mahfoud,^{†,‡} Il'ya A. Gural'skiy,^{†,§} William Nicolazzi,[†] Lionel Salmon,[†] Gábor Molnár,^{†,*} and Azzedine Bousseksou^{†,*}

[†]LCC, CNRS, and Université de Toulouse (UPS, INP), 205 route de Narbonne, F-31077 Toulouse, France

[‡]Optics & Photonics Center, Moroccan Foundation for Science, Innovation and Research, Technopolis Rabatshore, Morocco

[§]Department of Chemistry, National Taras Shevchenko University, 62 Vladimirskaya strasse, 01601 Kiev, Ukraine

S Supporting Information

ABSTRACT: Nano-objects and thin films displaying molecular spin-crossover phenomena have recently attracted much attention. However, the investigation of spin crossover at reduced sizes is still a big challenge. Here we demonstrate that surface plasmon polariton waves propagating along the interface between a metal and a dielectric layer can be used to detect the spin-state changes in the latter with high sensitivity, even at the nanometer scale.

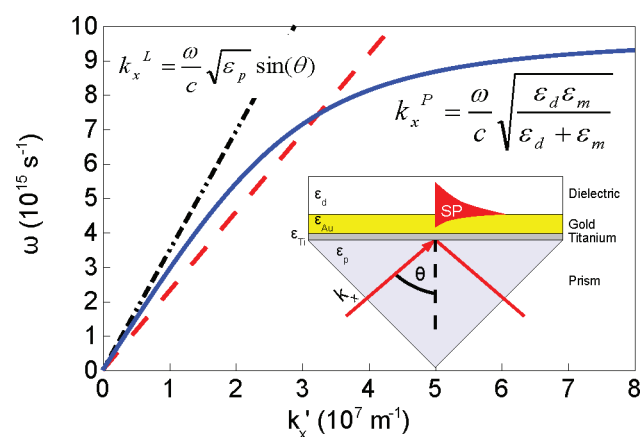
A number of (pseudo)octahedral 3d⁴–3d⁷ transition metal complexes have been reported to display a molecular bistability of their high-spin (HS) and low-spin (LS) electron configurations, which can be reversibly interconverted under external stimuli, such as temperature, pressure, magnetic field, or light irradiation.¹ This spin-crossover (SCO) phenomenon is accompanied by a spectacular change of magnetic, optical, dielectric, and mechanical properties.

In the past 5 years, we have been involved in a strong renewed interest in the SCO field, inspired by the emergence of nanosized SCO materials² such as coordination nanoparticles³ and continuous or nanopatterned thin films.⁴ In fact, bulk SCO materials exhibit in many cases strong electron–lattice coupling and associated cooperative phenomena, such as first-order phase transitions. The lowest size limit (assembly dimension) at which these cooperative effects are maintained turns into one of the key fundamental questions in this field. Beside the intriguing size-related properties, synthesizing thin films and other nanoscale assemblies of SCO complexes also represents a key step toward their technological applications in photonic and electronic devices.²

The SCO phenomenon has been investigated by various physical methods such as magnetic susceptibility and heat capacity measurements, X-ray diffraction, and Mössbauer, vibrational, and electronic spectroscopies.¹ These methods combined with different external stimuli provided a firm basis for understanding the physical mechanisms governing the spin-state switching in macroscopic materials (powder, single-crystal). However, these techniques become very limited for the investigation of SCO at the nanometer scale, and the development of new experimental approaches becomes indispensable.² In the present Communication, we show that surface plasmon resonance (SPR) is a very powerful tool to detect—even in nanometric layers—the refractive index change which accompanies the SCO phenomenon.

The field of plasmonics represents an exciting new area for the application of surface and nanoparticle plasmons (i.e., collective

Scheme 1. Dispersion Relation for Surface Plasmon Polaritons at the Metal–Dielectric Interface ($\omega-k_x^P$) Calculated for a Gold Film in Air (Continuous Line)^a



^a The dashed-dotted line is the dispersion relation for the exciting light wave without the prism, while the dashed line depicts the effect of the prism on the exciting light dispersion ($\omega-k_x^L$). The coupling of light with the surface plasmons can be achieved for a given value of ω by adjusting the angle of incidence (θ) in the attenuated total reflection (ATR) configuration as indicated in the inset.

oscillations of free electrons in metals) in nanotechnology.⁵ Here we focus on surface plasmon polaritons (SPPs), which are guided electromagnetic waves propagating at a metal–dielectric interface under light excitation. The coupling between the incident light and the plasmon polariton waves requires an intersection between their dispersion curves, i.e., simultaneous wavevector and frequency matching (Scheme 1). This can be achieved by means of a prism in the conventional “Kretschmann configuration”.⁶

If the wavelength is fixed (monochromatic light), SPR occurs at a given incident angle. The creation of the SPP wave causes an intensity loss in the angular reflectance spectrum of the incident light; the angle of the curve minimum is called the “plasmon resonance angle”, θ_{SPR} (see Figure 1 for an example). The location of this angle depends on the optical characteristics and thickness of the dielectric layer.⁶ This property, together with the fact that SPPs are strongly bound to the interface (only an evanescent tail

Received: August 1, 2011

Published: September 08, 2011

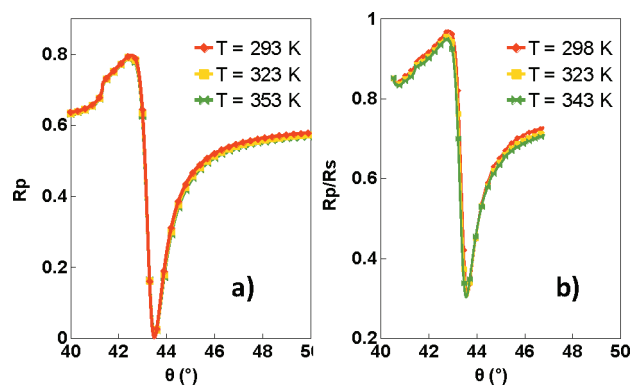


Figure 1. (a) Calculated and (b) experimental angular reflectance spectra at selected temperatures for a Ti/Au bilayer (5 nm Ti, 45 nm Au in air, $\lambda = 660$ nm).

penetrates into the films), provides a very interesting scope to investigate spin transitions in thin films by SPP-based techniques.

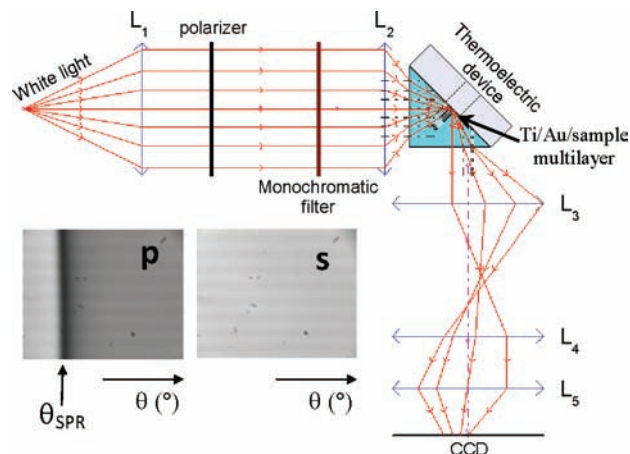
SPR curves were measured by using a custom-designed SPR setup (Scheme 2). A collimated white light beam is first polarized and monochromatized. The beam is then focused on the prism–metal interface. The reflected light beams are detected on different points of a CCD camera (1280 pixels with full vertical binning) according to their total internal reflection angle, θ . In a typical experiment, the spectrum range is $\Delta\theta = 6.3^\circ$ and the spectral resolution is 0.005° , but it is possible to adjust these values by using different lenses (L_4 , L_5). Since only light with p-polarization can excite a SPP, the reflectance curve with plasmon excitation (R_p) can be conveniently normalized by the reflectance curve with s-polarization (R_s) (see inset in Scheme 2).

Changes in molecular spin states can be induced most conveniently by changing the temperature of the material. In our SPR setup, this is achieved by bringing the SCO layer in contact with a Peltier device, in which a hole was drilled in order to keep air as the last dielectric layer. First we checked if the thermal variation of the optical constants of the prism and metal layers (Ti, Au) had an influence on our measurement. Figure 1 displays the calculated and experimentally observed temperature dependence of the reflectance spectra of a bilayer of titanium–gold in air for an interval of 60 K. The theoretical curves were calculated using the Fresnel equation and the conventional transfer matrix method (see the Supporting Information (SI) for further details).⁶ The optical constants of gold were taken from ref 7. The calculated and theoretical curves are in good agreement and indicate a negligible temperature dependence of the plasmon resonance angle within the investigated range (293–353 K).

In the next step we prepared a multilayer composed of 5 nm Ti, 45 nm Au, and 30 nm of the SCO complex $[\text{Fe}(\text{hptrz})_3](\text{OTs})_2$ (hptrz = 4-heptyl-1,2,4-triazole and OTs = tosylate) on a glass substrate, which was mounted on the “SPR prism” using an index-matching oil. We chose this SCO complex because its spin transition occurs just above room temperature, thus simplifying the study of the properties.⁸ (The structure of the complex as well as the synthesis details are provided in the SI.) AFM images (Figure 2) of the spin-coated films of $[\text{Fe}(\text{hptrz})_3](\text{OTs})_2$ reveal a homogeneous and smooth surface covering. The good quality of the films is an important asset so as to avoid spectral broadening and associated loss of resolution in the SPR measurements.

Figure 3a displays the angular reflectivity spectra recorded at two different temperatures, 303 and 336 K, for the multilayer

Scheme 2. Schematic Diagram of the Experimental SPR Setup^a



^aThe photos show typical CCD images for p- and s-polarized light reflected by the gold film on the back of the glass prism. The dark line (intensity loss) in the case of p-polarization is caused by the excitation of surface plasmons at the resonance angle θ_{SPR} .

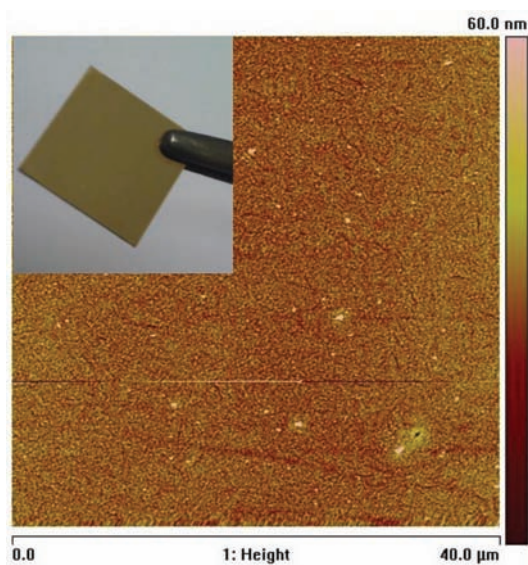


Figure 2. AFM image of a 30 nm thick $[\text{Fe}(\text{hptrz})_3](\text{OTs})_2$ film surface. The inset shows a photograph of the film on the glass/Ti/Au substrate.

glass/Ti (5 nm)/Au (45 nm)/ $[\text{Fe}(\text{hptrz})_3](\text{OTs})_2$ (30 nm). A clear shift of the “SPR dip” can be observed. The temperature dependence of the plasmon resonance angle is shown in Figure 3b. This curve is the result of two phenomena, thermal expansion and SCO, which are superimposed. On one hand, the thermal expansion of the complex leads to a decrease of the refractive index and thus the resonance angle decreases as well. In a not too large temperature range, heating of the material leads to a linear decrease of θ_{SPR} (see SI for further details). This is indeed what we observe in the low- and high-temperature sides in Figure 3b. One can notice that the slopes $d\theta_{\text{SPR}}/dT$ are different at low and high temperatures, which reflects the fact that the volumetric coefficient of thermal expansion ($\alpha = 1/V[\partial V/\partial T]$) is not the same in the LS and HS phases. On the other hand, most importantly, the thermal variation of θ_{SPR} reveals also a

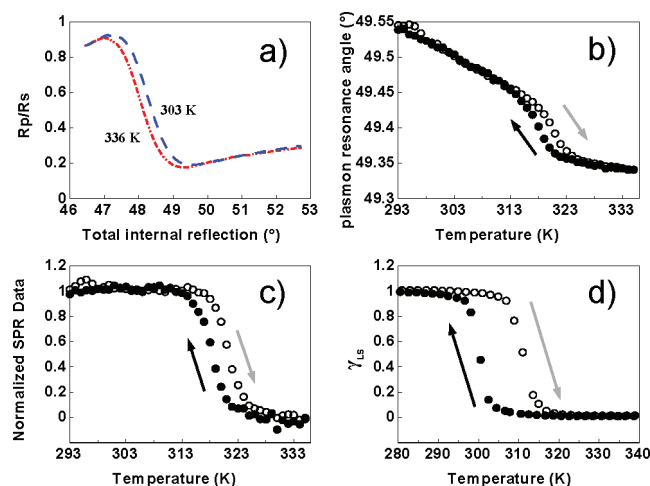


Figure 3. (a) Angle-dependent reflectance spectra of a glass/Ti (5 nm)/Au (45 nm)/[Fe(hptrz)₃](OTs)₂ (30 nm) multilayer at 303 K (LS state) and 336 K (HS state) ($\lambda = 660$ nm). (b) Temperature dependence of the plasmon resonance angle (reflectance minima) of the multilayer in the heating and cooling modes ($dT/dt = 2$ K/min). (c) The same data as in (b), but after correction for thermal dilatation and normalization. (d) Temperature dependence of the LS fraction of the bulk complex.

discontinuity around 320 K accompanied by a ~ 3 K wide hysteresis loop, which we can clearly assign to the spin transition. By subtracting the linear slopes, the SPR data can be normalized to obtain a curve which reflects solely the SCO phenomenon:

$$\theta_{\text{normalized}}(T) = [\theta_{\text{measured}}(T) - \theta_{\text{HS}}(T)] / [\theta_{\text{LS}}(T) - \theta_{\text{HS}}(T)]$$

The normalized curve in Figure 3c displaying the SCO behavior of the film can now be compared to the transition curve of the bulk microcrystalline sample (Figure 3d) measured by magnetometry. In both cases, the transition is first-order and accompanied by a hysteresis loop, but the transition temperatures and hysteresis widths are somewhat different ($T_{1/2}^{\uparrow} = 321$ K, $T_{1/2}^{\downarrow} = 318$ K for the film and $T_{1/2}^{\uparrow} = 311$ K, $T_{1/2}^{\downarrow} = 300$ K for the bulk). These differences may be attributed to either size reduction effects (increased surface-to-volume ratio) or slight alterations in the degree of hydration. Hydration of the sample leads to a shift of the transition temperature. This phenomenon is difficult to control because the sample is very hygroscopic. Moreover, the hydration rate of the bulk is certainly different when compared with that of the thin film; this is another fact that makes the bulk–film comparison difficult. A detailed study of the size reduction effects as well as the moisture sensing properties has been undertaken, but these questions are out of the scope of the present paper.

The results shown in Figure 3 prove clearly that SPPs can detect the SCO phenomenon in nanoscale thin films. Concerning the origin of the effect of SCO on the SPR signal, one should note that [Fe(hptrz)₃](OTs)₂ has a very low absorption coefficient in the visible range in both the HS and LS states (see SI for spectra). Moreover, around 660 nm—the wavelength used in the SPR measurements—the absorbance of the complex is the same in the two states. On the other hand, the change of the film thickness upon the SCO is expected to have an opposite effect on the SPR angle (see SI for further details). Therefore, the main parameter governing the reflectivity changes is the variation of the real part of the refractive index brought about by the SCO.

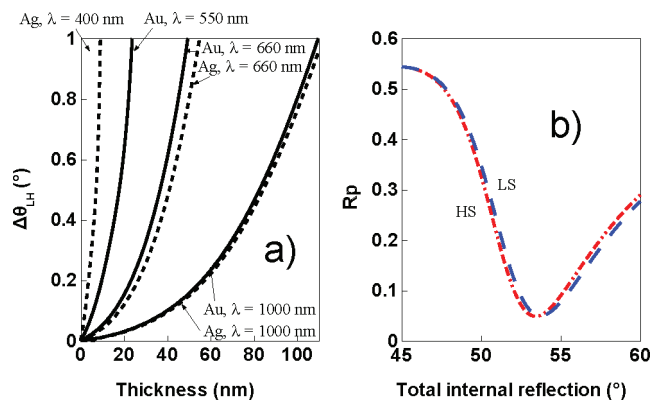


Figure 4. (a) Resonance angle shift associated with the SCO ($\Delta\theta_{\text{LH}}$) as a function of the thickness of the [Fe(hptrz)₃](OTs)₂ layer calculated for different wavelengths and support metals. (b) Calculated reflectance spectra ($\lambda = 400$ nm) of a glass/Ti (5 nm)/Ag (45 nm)/[Fe(hptrz)₃](OTs)₂ (5 nm) multilayer in the HS and LS states.

Using spectroscopic ellipsometry, we determined the refractive index of [Fe(hptrz)₃](OTs)₂ at room temperature ($n_{660\text{ nm}} = 1.5704$). Using this value, we extracted from the room-temperature SPR data the thickness of the [Fe(hptrz)₃](OTs)₂ layer (32 ± 3 nm). The good agreement with the AFM thickness data (30 ± 5 nm) provides strong proof for the validity of our SPR data treatment. The change of n associated with the spin-state change, $\Delta n_{\text{LH}} \approx 0.01$, was also determined from the SPR data (see SI). Since the electronic transitions in our compound have very weak oscillator strengths in the visible–near-infrared ranges, the electronic polarizability change of the cation upon the SCO must be rather small. Therefore, Δn_{LH} should be traced back primarily to the volume change accompanying the SCO (ΔV_{LH}), and the wavelength dependence of Δn_{LH} is expected to be relatively small in this case.

It is important to notice that the plasmon resonance angle is proportional to the refractive index of the SCO film, but the relationship between this refractive index and the HS/LS fractions ($\gamma_{\text{HS}}/\gamma_{\text{LS}}$) is not that simple. We used the Maxwell–Garnett effective medium approximation⁹ to determine the relative fraction of the two spin states (see SI). However, in the case of abrupt, discontinuous transitions, as for the present sample, the normalized SPR curve can be obviously assimilated with the $\gamma_{\text{LS}}(T)$ curve.

Using the experimentally determined value of Δn_{LH} , we carried out a series of theoretical simulations to determine the lowest size limit where the SPR technique can be used to detect the SCO phenomenon in this compound. Figure 4a displays the calculated plasmon resonance angle shifts ($\Delta\theta_{\text{LH}}$) due to the SCO as a function of the film thickness at different excitation wavelengths for both gold and silver metal layers. This shift is simulated by the change of the refractive index of the SCO material. From these simulations it is clear that one cannot define a set of optimum SPR parameters, but a few general rules can be sketched. For example, thick SCO layers should be studied using near-infrared excitation and gold support, while the investigation of ultrathin layers requires a silver layer and lower wavelength excitation.

As an example, Figure 4b shows the calculated reflectivity spectra for a 5 nm [Fe(hptrz)₃](OTs)₂ layer in the HS and LS states using a 45 nm silver support and 400 nm light excitation. The observed shift is around 0.3° , which is easily measurable with

our experimental setup. We shall note that with silver one can use lower excitation wavelengths with less penetration depth and thus higher surface sensitivity, and also the resonance peaks are sharper due to the smaller damping factor.⁶ On the other hand, silver is chemically less inert than gold, which might reduce its applicability in certain cases.

In summary, we have demonstrated experimentally that surface plasmon polaritons can be used to detect the spin-crossover phenomenon in nanometric thin films. The observed SPR angle shift was traced back to the refractive index change, which occurs primarily due to the volume change accompanying the SCO. This principle provides thus a generic detection method, which should be applicable for most SCO compounds and also in the case of other switchable molecular materials exhibiting a volume change (e.g., charge-transfer or Jahn–Teller switch). Using theoretical simulations, we have also shown that, by optimizing the experimental conditions, it should be possible to detect the spin-state changes down to at least 5 nm. One should note, however, that several SCO compounds show intense charge-transfer transitions in the visible range, and in such cases the strong absorbance change should lead to even lower SPR detection limits and also to a strong wavelength dependence. Vice versa, another interesting perspective of the present work is the possibility to use SCO thin films to modulate the propagation of electromagnetic waves in plasmonic or other type of guided wave devices. Potential applications include switches, tunable filters, mirrors, and chemical sensors.

■ ASSOCIATED CONTENT

S Supporting Information. Sample elaboration details, absorption spectra of $[\text{Fe}(\text{hptrz})_3](\text{OTs})_2$, details of the fitting of the SPR spectra, method of calculation of the refractive index and spin fractions, and discussion of dilation effects on the SPR signal. This material is available free of charge via the Internet at <http://pubs.acs.org>.

■ AUTHOR INFORMATION

Corresponding Author

gabor.molnar@lcc-toulouse.fr; azzedine.bousseksou@lcc-toulouse.fr

■ ACKNOWLEDGMENT

We acknowledge financial support from the project Cross-Nanomat (ANR-10-BLAN-716-1).

■ REFERENCES

- (1) Gütlich, P.; Goodwin, H., Eds. *Topics in Current Chemistry*, Vols. 233–235; 2004.
- (2) Bousseksou, A.; Molnár, G.; Salmon, L.; Nicolazzi, W. *Chem. Soc. Rev.* **2011**, *40*, 3313–3335.
- (3) (a) Forestier, T.; Mornet, S.; Daro, N.; Nishihara, T.; Mouri, S.-i.; Tanaka, K.; Fouche, O.; Freysz, E.; Létard, J.-F. *Chem. Commun.* **2008**, 4327–4329. (b) Coronado, E.; Galán-Mascarós, J. R.; Monrabal-Capilla, M.; García-Martínez, J.; Pardo-Ibáñez, P. *Adv. Mater.* **2007**, *19*, 1359–1361. (c) Tokarev, A.; Salmon, L.; Guari, Y.; Nicolazzi, W.; Molnár, G.; Bousseksou, A. *Chem. Commun.* **2010**, *46*, 8011–8013. (d) Volatron, F.; Catala, L.; Rivière, E.; Gloter, A.; Stephan, O.; Mallah, T. *Inorg. Chem.* **2008**, *47*, 6584–6586. (e) Larionova, J.; Salmon, L.; Guari, Y.; Tokarev, A.; Molvinger, K.; Molnár, G.; Bousseksou, A. *Angew. Chem., Int. Ed.* **2008**, *47*, 8236–8240. (f) Boldog, I.; Gaspar, A. B.; Martnez, V.;

Pardo-Ibanez, P.; Ksenofontov, V.; Battacharjee, A.; Gütlich, P.; Real, J. A. *Angew. Chem., Int. Ed.* **2008**, *47*, 6433–6437.

(4) (a) Cobo, S.; Molnár, G.; Real, J. A.; Bousseksou, A. *Angew. Chem., Int. Ed.* **2006**, *45*, 5786–5789. (b) Bodenthin, Y.; Pietsch, U.; Möhwald, H.; Kurth, D. G. *J. Am. Chem. Soc.* **2005**, *127*, 3110–3114. (c) Faulmann, C.; Chahine, J.; Malfant, I.; de Caro, D.; Cormary, B.; Valade, L. *Dalton Trans.* **2011**, *40*, 2480–2485. (d) Sereyuk, M.; Gaspar, A. B.; Ksenofontov, V.; Reiman, S.; Galyametdinov, Y.; Haase, E.; Rentschler, W.; Gütlich, P. *Chem. Mater.* **2006**, *18*, 2513–2515. (e) Matsuda, M.; Isozaki, H.; Tajima, H. *Thin Solid Films* **2008**, *517*, 1465–1467. (f) Cavallini, M.; Bergenti, I.; Milita, S.; Ruani, G.; Salitros, I.; Qu, Z.-R.; Chandrasekhar, R.; Ruben, M. *Angew. Chem., Int. Ed.* **2008**, *47*, 8596–8600. (g) Molnár, G.; Cobo, S.; Real, J. A.; Carcenac, F.; Daran, E.; Vieu, C.; Bousseksou, A. *Adv. Mater.* **2007**, *19*, 2163–2167. (h) Cavallini, M.; Bergenti, I.; Milita, S.; Kengne, J. C.; Gentili, D.; Ruani, G.; Salitros, I.; Meded, V.; Ruben, M. *Langmuir* **2011**, *27*, 4076–4081.

(5) Pitarke, J. M.; Silkin, V. M.; Chulkov, E. V.; Echenique, P. M. *Rep. Prog. Phys.* **2007**, *70*, 1–87.

(6) Schasfoort, R. B. M.; Tudos, A. J. *Handbook of Surface Plasmon Resonance*; Royal Society of Chemistry: Cambridge, 2008.

(7) (a) Palik, E. D. *Handbook of Optical Constants*, Vol. 1; Elsevier: Amsterdam, 1985. (b) Moreira, C. S.; Lima, A. M. N.; Neff, H.; Thirstrup, C. *Sens. Actuators B* **2008**, *134*, 854–862.

(8) Roubeau, O.; Alcazar Gomez, J. M.; Balskus, E.; Kolnaar, J. J. A.; Haasnoot, J. G.; Reedijk, J. *New J. Chem.* **2001**, *25*, 144–150.

(9) (a) Maxwell Garnett, J. C. *Philos. Trans. R. Soc. London A* **1904**, *203*, 385–420. (b) Ruppin, R. *Opt. Commun.* **2000**, *182*, 273–279.